

PAPER • OPEN ACCESS

Quantum noise cancellation in asymmetric speed metres with balanced homodyne readout

To cite this article: T Zhang *et al* 2018 *New J. Phys.* **20** 103040

View the [article online](#) for updates and enhancements.



IOP | ebooks™

Bringing you innovative digital publishing with leading voices to create your essential collection of books in STEM research.

Start exploring the collection - download the first chapter of every title for free.



PAPER

Quantum noise cancellation in asymmetric speed metres with balanced homodyne readout


OPEN ACCESS

RECEIVED
6 July 2018REVISED
27 September 2018ACCEPTED FOR PUBLICATION
15 October 2018PUBLISHED
29 October 2018

Original content from this work may be used under the terms of the [Creative Commons Attribution 3.0 licence](https://creativecommons.org/licenses/by/4.0/).

Any further distribution of this work must maintain attribution to the author(s) and the title of the work, journal citation and DOI.



T Zhang¹, E Knyazev² , S Steinlechner^{1,3}, F Ya Khalili^{4,5}, B W Barr¹, A S Bell¹ , P Dupej¹, J Briggs¹, C Gräf¹, J Callaghan¹, J S Hennig¹, E A Houston¹, S H Huttner¹, S S Leavey¹, D Pascucci¹, B Sorazu¹, A Spencer¹, J Wright¹, K A Strain¹, S Hild¹ and S L Danilishin^{1,6} 

¹ School of Physics and Astronomy, The University of Glasgow, Glasgow, G12 8QQ, United Kingdom

² LIGO, Massachusetts Institute of Technology, Cambridge, MA 02139, United States of America

³ Institut für Laserphysik und Zentrum für Optische Quantentechnologien der Universität Hamburg, Luruper Chaussee 149, D-22761 Hamburg, Germany

⁴ Faculty of Physics, M.V. Lomonosov Moscow State University, 119991 Moscow, Russia

⁵ Russian Quantum Center, 143025 Skolkovo, Russia

⁶ Institut für Theoretische Physik/Institut für Gravitationsphysik (Albert-Einstein-Institut), Leibniz Universität Hannover, Callinstraße 38, D-30167 Hannover, Germany

E-mail: stefan.danilishin@ligo.org

Keywords: balanced homodyne detector, speed metre, quantum noise

Abstract

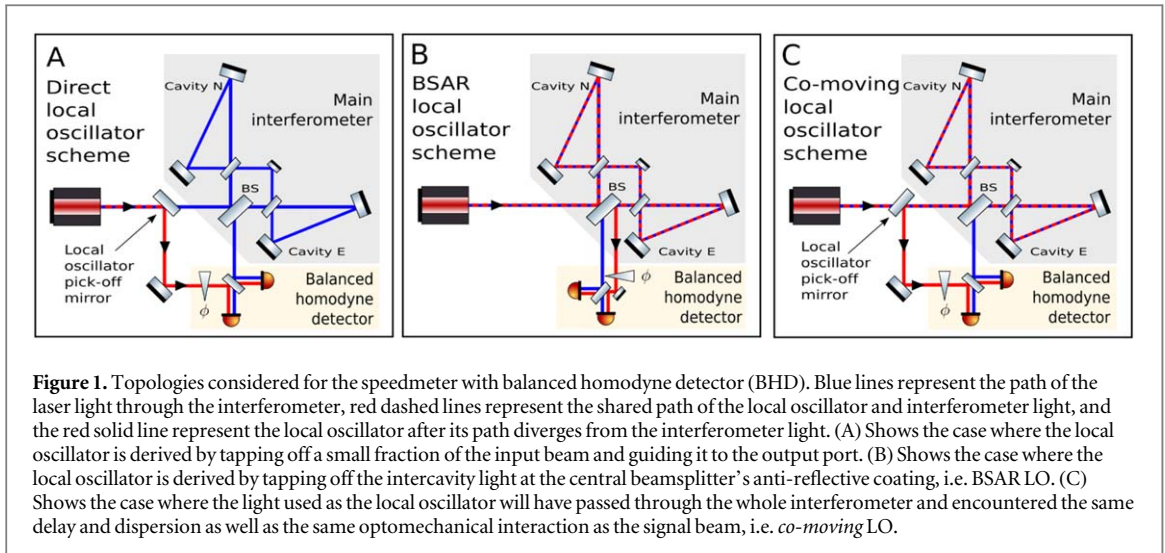
The Sagnac speed metre topology has been identified as a promising technique to reduce quantum back-action in gravitational-wave interferometers. However, imbalance of the main beamsplitter has been shown to increase the coupling of laser noise to the detection port, thus reducing the quantum noise superiority of the speed metre, compared to conventional approaches, in particular at low frequencies. In this paper, we show that by implementing a balanced homodyne readout scheme with a suitable choice of the point from which the local oscillator (LO) is derived, the excess laser noise contribution is partly compensated, and the resulting speed metre can be more sensitive than state-of-the-art position metres. This is achieved by picking-off the LO from either the reflection port of the interferometer or the anti-reflective coating surface of the main beamsplitter. We show that either approach relaxes the relative intensity noise (RIN) requirement of the input laser. For example, for a beam splitter imbalance of 0.1% in the Glasgow speed metre proof of concept experiment, the RIN requirement at frequency of 100 Hz decreases from $4 \times 10^{-10}/\sqrt{\text{Hz}}$ to $4 \times 10^{-7}/\sqrt{\text{Hz}}$, moving the RIN requirement from a value that is hard to achieve in practice, to one which is routinely obtained.

1. Introduction

In 2015, we stepped into the era of gravitational-wave astronomy with the first direct detection of gravitational waves (GW) from a colliding binary black hole (BBH) system by the two Advanced LIGO interferometers [1]. Two exciting years of discoveries have given us four more BBH merger events [2–5], and one collision of neutron stars [6], with the last system also being observed in the electromagnetic spectrum [7].

Those discoveries, apart from generating a great deal of fascinating new science hitherto unavailable to humanity, identified the need to improve the sensitivity of the existing detectors, particularly in the low frequency range (<30 Hz) where the noise of the detector masks GW signals from massive black holes, i.e. with masses $>30M_{\odot}$, where M_{\odot} is one solar mass. It also masks GWs from a stage in the evolution of binary neutron stars a few minutes before the end of the in-spiral, observation of which could allow an early warning to be issued to EM observers.

The design sensitivity of current and proposed laser interferometric gravitational-wave detectors is limited by quantum noise [8, 9] over much of their detection frequency band. This noise stems from fundamental quantum-mechanical fluctuations of the phase and amplitude of coherent laser light. In particular, amplitude fluctuations which produce a random back-action force on the test masses, will mimic the action of GWs when



the power in the arms reaches the design level of MW and could therefore have the largest potential impact at low frequencies where the noise amplitude rises as f^{-2} , in which f is the GW frequency.

Speed-metre interferometers were first proposed by Braginsky and Khalili [10] as a way to suppress quantum back-action noise in bar GW detectors. Later, this concept was generalised to laser GW interferometers [11]. Back-action noise reduction in speed metres stems from the quantum non-demolition (QND) nature of test mass' velocity [12] as a quantum observable, in contrast to the displacement measured by Michelson interferometers. This advantage of speed metres over position metres at low frequencies inspired the development of several different speed metre topologies [13–18].

One of these configurations, the zero-area Sagnac interferometer, was first identified as a QND speed-metre by Chen [14]. In a Sagnac interferometer, two counter-propagating light beams visit the arms sequentially in the opposite order and return to the main beam-splitter. In this process, each beam carries phase information resulting from mirror displacements in both arms but the light visits the two arms at times separated by the interval τ , equal to the arm cavity ring down time. The counter-propagating beams add at the beamsplitter and interfere destructively at the readout port of the interferometer. Detection of this light results in an output signal which carries phase information proportional to the mean relative velocity of the interferometer arm length changes. Hence the Sagnac interferometer performs a QND measurement of speed.

In the ideal case, a Sagnac interferometer is always operating at the dark fringe at DC. Only signal sidebands, with amplitude proportional to the relative differential velocity described above, propagate to the readout port. This robustness of Sagnac topology to optical path variations, compared to the usual Michelson interferometer, was deemed to be an advantage, warranting its application in GW detectors [19]. However, it was later recognised that any deviation of the main beamsplitter from the ideal 50:50 ratio would pose a limit to the sensitivity that could be achieved, due to coupling of laser-port fluctuations to the readout port [20, 21].

It has been shown that by adding appropriate readout methods to speedmeter interferometers, it is possible to reduce the coupling of laser noise fluctuations to the GW readout signal [20, 22, 23]. In this paper we take inspiration from that work, and analytically investigate the potential cancellation of quantum noise in asymmetric (i.e. non-ideal) Sagnac speedmeters that employ balanced homodyne detectors. By extending this analysis to the Glasgow Sagnac speed metre (SSM), we investigate potential additional cancellation of laser technical noise.

The Glasgow SSM employs balanced homodyne readout and we show three options for the arrangement of the required local oscillator (LO) in figure 1. We examine the quantum and classical noise reduction when using a balanced homodyne detector LO taken from the interferometer bright port (BP) versus the noisier option of using laser light which has not been through the interferometer. Given the partial cancellation of laser noise, we can allow for deviation from 50:50 ratio at the main beamsplitter and thus resolve the primary problem that has been identified with Sagnac interferometers.

In section 2, we conduct an analytical treatment of quantum noise of an asymmetric SSM interferometer, and show how balanced homodyne readout can help to suppress quantum noise, given the proper choice of the LO. In section 3 we show the analysis on the relaxed requirement of relative laser intensity noise based on simulation software FINESSE [24].

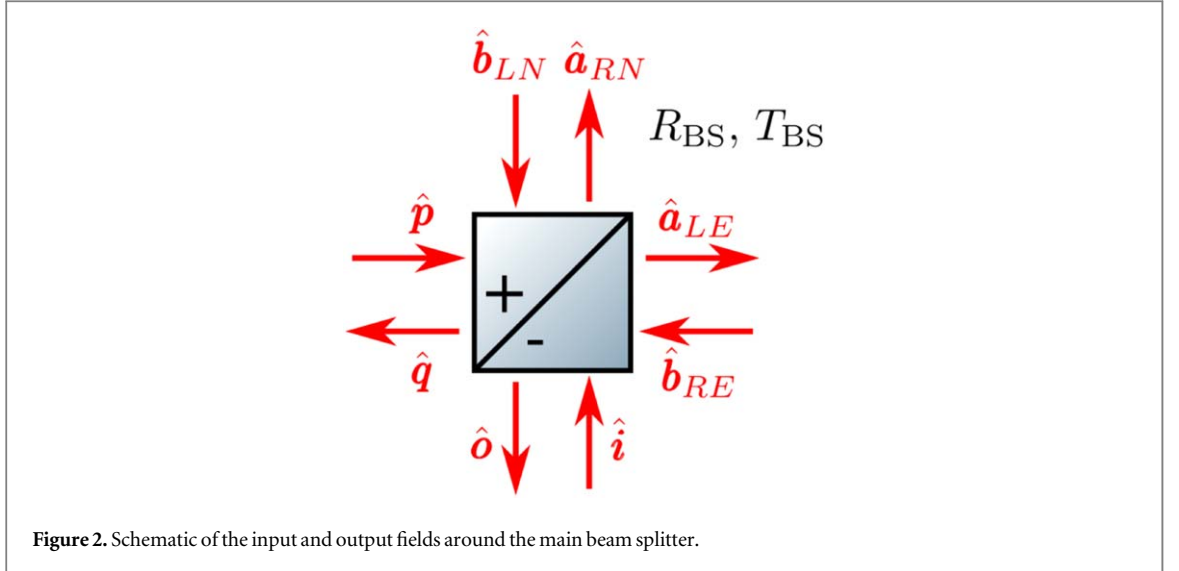


Figure 2. Schematic of the input and output fields around the main beam splitter.

2. Quantum noise of an imperfect speedmeter IFO

2.1. Two-photon formalism

In this section, we use the two-photon formalism of quantum optics [25, 26]. It describes, locally, an arbitrary quasi-monochromatic modulated electromagnetic wave with strain $\hat{E}(t) = \mathcal{E}_0[(A_c + \hat{a}_c(t))\cos \omega_p t + (A_s + \hat{a}_s(t))\sin \omega_p t]$ in terms of two-dimensional vectors of quadrature amplitudes $\mathbf{A} + \hat{\mathbf{a}}$, where $\mathbf{A} = \{A_c, A_s\}^T$ stands for DC mean amplitudes vector and $\hat{\mathbf{a}} = \{\hat{a}_c, \hat{a}_s\}^T$ stands for zero-mean non-stationary variations and fluctuations of light (superscript T denotes transpose of the matrix or vector). Here normalisation constant $\mathcal{E}_0 = \sqrt{\frac{4\pi\hbar\omega_p}{\mathcal{A}}}$, \mathcal{A} is effective cross section of the beam, c the speed of light, and ω_p is the carrier light frequency. It is usually more convenient to work in the frequency domain:

$$\hat{a}_{c,s}(t) = \int_{-\infty}^{\infty} \frac{d\Omega}{2\pi} \hat{a}_{c,s}(\Omega) e^{-i\Omega t}, \quad (1)$$

where we define quadratures spectra at the modulation sidebands off-set frequency $\Omega = \omega - \omega_p$.

In order to understand how the fluctuations entering the pumping port of the interferometer influence all three variants, we need to analyse the input–output relations of the asymmetric interferometer with an emphasis on the transfer functions of the pump sideband fields to both, the readout port, and to the LO. Hereinafter we attain the result.

2.2. Input–output relations of the asymmetric Sagnac interferometer

We consider a Sagnac interferometer with main beam splitter non-unity ratio $R_{BS}/T_{BS} \neq 1$. The beam splitter is depicted in figure 2, with R_{BS} and T_{BS} representing the power reflectivity and transmissivity of the main beam splitter. The three LO choices that we investigate here require the knowledge of the following 3 output fields,

- (i) Readout port output field \hat{o} (for all three variants)
- (ii) Part \hat{b}^{RE} of the output field \hat{o} contributed by the clockwise propagating light beam that gives the LO field upon reflection off the main beam splitter anti-reflecting coating (variant figure 1(B))
- (iii) Return field \hat{q} at the pumping port (for the *co-moving* LO choice of figure 1(C))

Expressed in terms of the dark port (DP) input field, \hat{i} and BP input field \hat{p} and signal displacements. Following the [21], those can be written as:

$$\hat{o} = \mathbb{T}_i \hat{i} + \mathbb{T}_p \hat{p} + \mathbf{t}_d x_d + \mathbf{t}_c x_c, \quad (2)$$

$$\hat{q} = \mathbb{R}_i \hat{i} + \mathbb{R}_p \hat{p} + \mathbf{q}_d x_d + \mathbf{q}_c x_c, \quad (3)$$

$$\hat{b}^{RE} = \mathbb{T}_i^{RE} \hat{i} + \mathbb{T}_p^{RE} \hat{p} + \mathbf{t}_d^{RE} x_d + \mathbf{t}_c^{RE} x_c, \quad (4)$$

where $x_c = x_n + x_e$ and $x_d = x_n - x_e$ stand for the two mechanical modes of the Sagnac interferometer, namely the *common* and the *differential* arm elongation modes or cARM mode and dARM mode. The transfer matrices

\mathbb{T}_i , \mathbb{T}_i^{RE} and \mathbb{R}_i define the coupling of DP input field \hat{i} to the corresponding output port. The other three matrices are of more interest to us, i.e. \mathbb{T}_p , \mathbb{T}_p^{RE} and \mathbb{R}_p , as they describe how laser fluctuations \hat{p} couple to the corresponding output ports of the interferometer. It is straightforward to show (see [21] for details) that these transfer matrices, in case of imbalanced beam splitter with $R_{\text{BS}} \neq T_{\text{BS}}$, follow the well known structure of the tuned optomechanical interferometer transfer matrix (see, e.g., [27, 28]):

$$\mathbb{T}_i = 2\sqrt{R_{\text{BS}}T_{\text{BS}}}e^{2i\beta_{\text{sag}}}\begin{bmatrix} 1 & 0 \\ -\mathcal{K}_{\text{sym}} & 1 \end{bmatrix}, \quad (5)$$

$$\mathbb{R}_i = (R_{\text{BS}} - T_{\text{BS}})e^{2i\beta_{\text{sag}}}\begin{bmatrix} 1 & 0 \\ 0 & 1 \end{bmatrix}, \quad (6)$$

$$\mathbb{T}_p = (R_{\text{BS}} - T_{\text{BS}})e^{2i\beta_{\text{sag}}}\begin{bmatrix} 1 & 0 \\ -4\mathcal{K}_{\text{arm}} & 1 \end{bmatrix}, \quad (7)$$

$$\mathbb{R}_p = -2\sqrt{R_{\text{BS}}T_{\text{BS}}}e^{2i\beta_{\text{sag}}}\begin{bmatrix} 1 & 0 \\ -\mathcal{K}_{\text{asym}} & 1 \end{bmatrix}, \quad (8)$$

$$\mathbb{T}_i^{\text{RE}} = \sqrt{T_{\text{BS}}}e^{2i\beta_{\text{sag}}}\begin{bmatrix} 1 & 0 \\ -2R_{\text{BS}}\mathcal{K}_{\text{sym}} & 1 \end{bmatrix}, \quad (9)$$

$$\mathbb{T}_p^{\text{RE}} = \sqrt{R_{\text{BS}}}e^{2i\beta_{\text{sag}}}\begin{bmatrix} 1 & 0 \\ 4\mathcal{K}_{\text{arm}} - 2T_{\text{BS}}\mathcal{K}_{\text{sym}} & 1 \end{bmatrix}, \quad (10)$$

with diagonal elements describing the purely optical response (with fixed mirrors position), whereas the lower off-diagonal term, featuring the so called optomechanical coupling factor \mathcal{K} first introduced by Kimble *et al* [27], embraces the details of interaction of mechanical degrees of freedom of the interferometer with the corresponding light field (via radiation pressure). Response of the interferometer to both, differential and common mechanical motion of the mirrors can be written as:

$$\mathbf{t}_d = -e^{i\beta_{\text{sag}}}\frac{\sqrt{2\mathcal{K}_{\text{sym}}}}{x_{\text{SQL}}}\begin{bmatrix} 0 \\ 1 \end{bmatrix}, \quad (11)$$

$$\mathbf{t}_c = ie^{i\beta_{\text{sag}}}\frac{(R_{\text{BS}} - T_{\text{BS}})\sqrt{2\mathcal{K}_{\text{asym}}}}{x_{\text{SQL}}}\begin{bmatrix} 0 \\ 1 \end{bmatrix}, \quad (12)$$

$$\mathbf{t}_d^{\text{RE}} = e^{i\beta_{\text{sag}}}\frac{\sqrt{2R_{\text{BS}}\mathcal{K}_{\text{sym}}}}{x_{\text{SQL}}}\begin{bmatrix} 0 \\ 1 \end{bmatrix}, \quad (13)$$

$$\mathbf{t}_c^{\text{RE}} = -ie^{i\beta_{\text{sag}}}\frac{\sqrt{2R_{\text{BS}}\mathcal{K}_{\text{asym}}}}{x_{\text{SQL}}}\begin{bmatrix} 0 \\ 1 \end{bmatrix}, \quad (14)$$

$$\mathbf{q}_d = \begin{bmatrix} 0 \\ 0 \end{bmatrix}, \quad (15)$$

$$\mathbf{q}_c = -e^{i\beta_{\text{sag}}}\frac{2\sqrt{2R_{\text{BS}}T_{\text{BS}}\mathcal{K}_{\text{asym}}}}{x_{\text{SQL}}}\begin{bmatrix} 0 \\ 1 \end{bmatrix}, \quad (16)$$

where $\beta_{\text{sag}} = 2\beta_{\text{arm}} + \frac{\pi}{2}$ is the Sagnac-specific additional phase shift that signal sidebands at frequency Ω acquire in the course of propagation through the interferometer. $x_{\text{SQL}} = \sqrt{\frac{2\hbar}{M\Omega^2}}$ stands for the free mass displacement standard quantum limit (SQL). Symmetric and asymmetric optomechanical coupling factors of imperfect Sagnac interferometer are defined the same way as in [21]:

$$\mathcal{K}_{\text{sym}} = 4\mathcal{K}_{\text{arm}}\sin^2\beta_{\text{arm}} \simeq \frac{8\Theta_{\text{arm}}\gamma_{\text{arm}}}{(\Omega^2 + \gamma_{\text{arm}}^2)^2}, \quad (17)$$

$$\mathcal{K}_{\text{asym}} = 4\mathcal{K}_{\text{arm}}\cos^2\beta_{\text{arm}} \simeq \frac{8\Theta_{\text{arm}}\gamma_{\text{arm}}^3}{\Omega^2(\Omega^2 + \gamma_{\text{arm}}^2)^2}. \quad (18)$$

with $\beta_{\text{arm}} = \arctan\frac{\Omega}{\gamma_{\text{arm}}}$ the phase shift acquired by a sideband field in one arm cavity. $\gamma_{\text{arm}} = \frac{cT_{\text{ITM}}}{4L}$ is the half-bandwidth of the arm cavities with length L and input mirror power transmissivity T_{ITM} .

$\mathcal{K}_{\text{arm}} = \frac{2\Theta\gamma_{\text{arm}}}{\Omega^2(\gamma_{\text{arm}}^2 + \Omega^2)}$ is the optomechanical coupling factor of this arm with $\Theta = \frac{4\omega_p P_{\text{arm}}}{McL}$ the normalised power, where P_{arm} is the circulating in each arm of an equivalent Michelson, M is the reduced mass of the dARM mode and L is the length of the arm. Note that $\mathcal{K}_{\text{sym}} + \mathcal{K}_{\text{asym}} = 4\mathcal{K}_{\text{arm}}$, which will be used later.

2.3. Balanced homodyne readout

One sees that asymmetry of the BS couples a fraction of pump laser light to the DP of the interferometer. This creates a non-zero DC component of the signal light (i.e. a component at the carrier frequency) that can be easily obtained from the I/O-relations above if one sets $\Omega \rightarrow 0$ and $\mathcal{K}_{\text{arm}} \rightarrow 0$,

$$\mathbf{O} = (R_{\text{BS}} - T_{\text{BS}})\mathbf{P}, \quad (19)$$

where the corresponding DC fields are expressed in terms of pump field at the main BS, \mathbf{P} . Analogously, one can derive the DC component of the LO beam for all three choices of the LO.

- (i) $L_{\text{dir}} \propto \mathbf{P}$ for the direct LO option;
- (ii) $L_{\text{AR}} \propto \mathbf{B}^{\text{RE}} \propto \sqrt{R_{\text{BS}}}\mathbf{P}$ for the BS AR coating reflection LO option;
- (iii) $L_{\text{co}} \propto \mathbf{Q} \propto -2\sqrt{R_{\text{BS}}T_{\text{BS}}}\mathbf{P}$ for the *co-moving* LO option;

As shown in [29, 30], the fluctuation part of the readout photocurrent of the balanced homodyne detector is proportional to a sum of following terms:

$$I_{\text{HD}} \propto \hat{\mathbf{o}}^\dagger \mathbb{H} \hat{\mathbf{L}} + \mathbf{O}^T \mathbb{H} \hat{\mathbf{I}}, \quad (20)$$

where

$$\mathbb{H} = \begin{bmatrix} \cos \phi & -\sin \phi \\ \sin \phi & \cos \phi \end{bmatrix}, \quad (21)$$

with ϕ defining the homodyne angle. $\hat{\mathbf{I}}$ stands for the noise fields of the LO. For $\phi = \pi/2$ (phase quadrature readout), the photocurrent can be further simplified as

$$I_{\text{HD}} \propto |\mathbf{L}| \hat{o}_s - |\mathbf{O}| \hat{I}_s, \quad (22)$$

The potential of noise cancellation can be readily seen from this expression, for the phase noise in the two optical paths comes from the same source, i.e. from the pump laser. Following we continue to demonstrate how the quantum noise cancellation is tailored by properly choosing the LO delivery port. The $\hat{\mathbf{I}}$ field for three choices of the LO we consider here can be written along the same lines as corresponding classical amplitudes of the LO \mathbf{L} :

- (i) $\hat{\mathbf{I}}_{\text{dir}} \propto \hat{\mathbf{p}}$ for the direct LO option;
- (ii) $\hat{\mathbf{I}}_{\text{AR}} \propto \hat{\mathbf{b}}^{\text{RE}}$ for the BS AR coating reflection LO option;
- (iii) $\hat{\mathbf{I}}_{\text{co}} \propto \hat{\mathbf{q}}$ for the *co-moving* LO option.

At low frequencies, the main contribution to the quantum noise comes from the off-diagonal radiation pressure term in the transfer matrices, as \mathcal{K}_{arm} and $\mathcal{K}_{\text{asym}}$ both rise steeply as $\Omega \rightarrow 0$. Indeed, we substitute equations (2), (3) into equation (20), leaving only the leading terms, one can get the low-frequency contribution to the readout photocurrent from BP for the *co-moving* LO option the following expression:

$$I_{\text{co}}^{\text{BP}} \propto \mathcal{I}_{\text{co}}[(4\mathcal{K}_{\text{arm}} - \mathcal{K}_{\text{asym}})\sin \phi - 2\cos \phi] \hat{p}_c = \mathcal{I}_{\text{co}}[\mathcal{K}_{\text{sym}}\sin \phi - 2\cos \phi] \hat{p}_c. \quad (23)$$

Similarly, for BSAR LO option one can get:

$$I_{\text{BSAR}}^{\text{BP}} \propto \mathcal{I}_{\text{BSAR}}[\mathcal{K}_{\text{sym}}\sin \phi - 2\cos \phi] \hat{p}_c, \quad (24)$$

where

$$\mathcal{I}_{\text{co}} = 2\sqrt{R_{\text{BS}}T_{\text{BS}}}(R_{\text{BS}} - T_{\text{BS}})e^{2i\beta_{\text{sag}}}\mathbf{P}, \quad (25)$$

$$\mathcal{I}_{\text{BSAR}} = 2\sqrt{R_{\text{BS}}T_{\text{BS}}}(T_{\text{BS}} - R_{\text{BS}})e^{2i\beta_{\text{sag}}}\mathbf{P}. \quad (26)$$

With homodyne angle $\phi = \pi/2$, we simply have

$$I^{\text{BP}} \propto \mathcal{K}_{\text{sym}} \hat{p}_c, \quad (27)$$

for both the *co-moving* LO and the LO derived from the BSAR coating reflection. This expression shows partial cancellation of steep low-frequency dependence and only the *speed-metre-like* term remains, which manifests in flat low-frequency dependence. This remaining term, as we discuss later, stems from the differential back-action force driven by the BP amplitude fluctuations represented by a cosine quadrature operator \hat{p}_c . Even though, since this remaining term is proportional to $|R_{\text{BS}} - T_{\text{BS}}|$ which refers to the beam splitter asymmetry, as shown in equations (25), (26), its contribution is always much smaller than the quantum noise contribution from DP in terms of any realistic beam splitter imbalance. However, for LO derived directly from main laser, the expression has no radiation pressure related contribution in the second term in equation (20), hence

$$I_{\text{dir}}^{\text{BP}} \propto \mathcal{K}_{\text{arm}} \hat{p}_c, \quad (28)$$

and the contribution from the BP-driven common motion of the interferometer mirrors remains uncompensated.

The physics behind this cancellation stems from the very principle of the balanced homodyne readout, where any fluctuations and variations of light that drive both, the LO and the signal light in the same way, are cancelled by design. Hence the partial cancellation of quantum noise that we demonstrated above comes from this insensitivity to the common phase signal produced by the common part of the radiation pressure force, created by the BP fluctuations \hat{p} , i.e. $\hat{F}_c^{\text{r.p.}} = (\hat{F}_n^{\text{r.p.}} + \hat{F}_e^{\text{r.p.}})/2$ where $\hat{F}_{e,n}^{\text{r.p.}}$ stand for radiation pressure forces in each of the arms. The remaining uncompensated part stems from the non-zero differential radiation pressure force, $\hat{F}_d^{\text{r.p.}} = (\hat{F}_n^{\text{r.p.}} - \hat{F}_e^{\text{r.p.}})/2$, ensuing from the imbalance of the amplitudes of the reflected and transmitted light at the asymmetric main beam-splitter.

2.4. Quantum noise limited sensitivity of Sagnac interferometer with BP noise cancellation

It is straightforward now to calculate the QNLS power spectral density expressions for all three choices of LO, using the derived earlier I/O-relations for both, the BP and the DP of the interferometer. It requires knowing the transfer matrices of the BHD photocurrent in all three considered schemes on the input fluctuation fields, \hat{i} and \hat{p} . In order to simplify the equation, the rotation matrix \mathbb{H} is absorbed into \mathbf{L} and \mathbf{O} . After expressing the LO fluctuations field, $\hat{\mathbf{I}}$, in terms of \hat{i} and \hat{p} one gets from (20):

$$\hat{I}_{\text{dir}} \propto \mathbf{L}_{\text{dir}}^T \mathbb{T}_i \hat{i} + (\mathbf{L}_{\text{dir}}^T \mathbb{T}_p + \mathbf{O}^T) \hat{p} + t_d^{\text{dir}} x_d + t_c^{\text{dir}} x_c, \quad (29)$$

$$\hat{I}_{\text{co}} \propto (\mathbf{L}_{\text{co}}^T \mathbb{T}_i + \mathbf{O}^T \mathbb{R}_i) \hat{i} + (\mathbf{L}_{\text{co}}^T \mathbb{T}_p + \mathbf{O}^T \mathbb{R}_p) \hat{p} + t_d^{\text{co}} x_d + t_c^{\text{co}} x_c, \quad (30)$$

$$\hat{I}_{\text{BS,AR}} \propto (\mathbf{L}_{\text{AR}}^T \mathbb{T}_i + \mathbf{O}^T \mathbb{T}_i^{\text{RE}}) \hat{i} + (\mathbf{L}_{\text{AR}}^T \mathbb{T}_p + \mathbf{O}^T \mathbb{T}_p^{\text{RE}}) \hat{p} + t_d^{\text{AR}} x_d + t_c^{\text{AR}} x_c, \quad (31)$$

where the last two terms stand for the signal part of the BHD photocurrent caused by the differential and common signal motion of the mirrors, respectively. For the general case of arbitrary homodyne angle, ϕ_{LO} , the corresponding expressions for the dARM and cARM responses in all three cases read:

$$t_d^{\text{dir}} = i e^{i\beta_{\text{sag}}} \frac{\sqrt{2\mathcal{K}_{\text{sym}}}}{x_{\text{SQL}}} \sin \phi_{\text{LO}}, \quad t_c^{\text{dir}} = e^{i\beta_{\text{sag}}} (R_{\text{BS}} - T_{\text{BS}}) \frac{\sqrt{2\mathcal{K}_{\text{asym}}}}{x_{\text{SQL}}} \sin \phi_{\text{LO}}, \quad (32)$$

$$t_d^{\text{co}} = i e^{i\beta_{\text{sag}}} \frac{\sqrt{8R_{\text{BS}} T_{\text{BS}} \mathcal{K}_{\text{sym}}}}{x_{\text{SQL}}} \sin \phi_{\text{LO}}, \quad t_c^{\text{co}} = 0, \quad (33)$$

$$t_d^{\text{AR}} = i e^{i\beta_{\text{sag}}} \frac{\sqrt{8R_{\text{BS}} (T_{\text{BS}})^2 \mathcal{K}_{\text{sym}}}}{x_{\text{SQL}}} \sin \phi_{\text{LO}}, \quad t_c^{\text{AR}} = 0. \quad (34)$$

Note that for the *co-moving* LO and for the BS AR-coating reflected LO there is an additional advantage of zero sensitivity to the common motion of the arms (cARM degree of freedom). It cuts off the potential coupling of noise from the much loosely controlled cARM degree of freedom into the readout channel of the Sagnac interferometer. Finally, one can calculate the QNLS power spectral density of a Sagnac interferometer, in the units of differential displacement of the arms using the following well-known general formula:

$$S_{\text{LO option}}^x = \frac{\langle in | \hat{L}_{\text{LO option}}(\Omega) \circ \hat{L}_{\text{LO option}}(\Omega') | in \rangle}{|t^{\text{LO option}}|}. \quad (35)$$

The general formula reads:

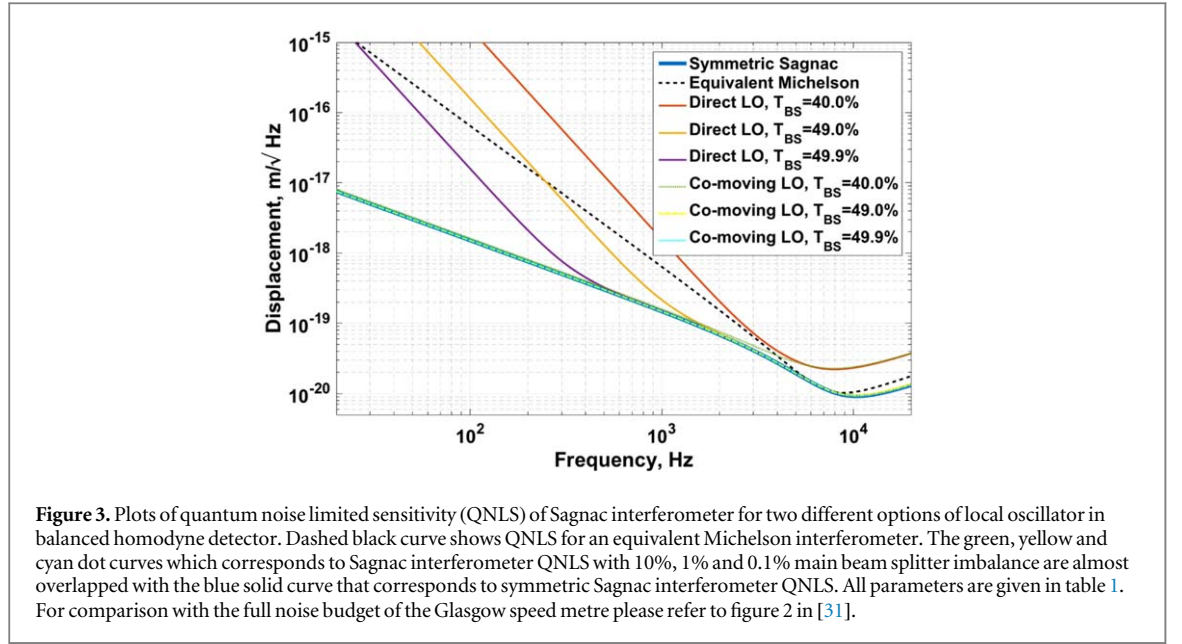
$$\begin{aligned} S_{\text{co}}^x(\Omega) &= S_{\text{DP,co}}^x + S_{\text{BP,co}}^x + S_{\text{PO,co}}^x \\ &= \frac{(\mathbf{L}^T \mathbb{T}_i + \mathbf{O}^T \mathbb{R}_i) \mathbb{S}^i (\mathbb{T}_i^{\dagger} \mathbf{L} + \mathbb{R}_i^{\dagger} \mathbf{O})}{|\mathbf{L}^T \mathbf{t}_d|^2} + \frac{(\mathbf{L}^T \mathbb{T}_p + \mathbf{O}^T \mathbb{R}_p) \mathbb{S}^p (\mathbb{T}_p^{\dagger} \mathbf{L} + \mathbb{R}_p^{\dagger} \mathbf{O})}{|\mathbf{L}^T \mathbf{t}_d|^2} + \frac{T_p \mathbf{O}^T \mathbf{O}}{|\mathbf{L}^T \mathbf{t}_d|^2}, \end{aligned} \quad (36)$$

where we assumed that the power reflectivity/transmissivity of the pick-off beam splitter is equal to R_p/T_p and there is an additional noise term, S_{PO}^x due to vacuum fields, entering the open port of this beam splitter. Here \mathbb{S}^a is the spectral density matrix for the input light $\hat{\mathbf{a}}(\Omega)$, defined as

$$2\pi \mathbb{S}_{ij}^a(\Omega) \delta(\Omega - \Omega') = \langle \text{vac} | \hat{a}_i(\Omega) \circ \hat{a}_j^{\dagger}(\Omega') | \text{vac} \rangle, \quad (37)$$

where averaging goes over the vacuum quantum state of light $|\text{vac}\rangle$ and $\{i, j\} = \{c, s\}$. Substitution of (5) and (11) gives for the components of the QNLS the following formulae:

$$S_{\text{DP,co}}^x = \frac{x_{\text{SQL}}^2}{2} \frac{1 + [\mathcal{K}_{\text{sym}}^* - (8R_{\text{BS}} T_{\text{BS}} - 1) \cot \phi_{\text{LO}}]^2}{\mathcal{K}_{\text{sym}}^*}, \quad (38)$$



$$S_{BP,co}^x = \frac{x_{SQL}^2 (R_{BS} - T_{BS})^2 [\mathcal{K}_{sym} - 2 \cot \phi_{LO}]^2}{2 \mathcal{K}_{sym}}, \quad (39)$$

$$S_{PO,co}^x = \frac{x_{SQL}^2 T_p (R_{BS} - T_{BS})^2}{2 R_p \mathcal{K}_{sym}^* \sin^2 \phi_{LO}}, \quad (40)$$

where $\mathcal{K}_{sym}^* = 4R_{BS}T_{BS}\mathcal{K}_{sym}$ is the new effective optomechanical coupling factor with account for BS asymmetry. The suppression of noise due to the double measurement scheme of the SSM and BHD, the *speedmeter frequency dependence* of the quantum noise at low frequencies, is seen in figure 3.

3. Relative laser intensity noise requirement

The direct implication of suppression of laser noise contribution to the QNLS, discussed earlier and shown in figure 3, is the much relaxed relative laser intensity noise (RIN) requirements, ensuing from the significantly weakened transfer function from BP amplitude quadrature to the BHD readout following from the equations (27) and (28).

In this section, we consider as an example the SSM proof-of-principle experiment being built in the University of Glasgow [31]. Due to the complexity of the instrument, we have eschewed analytical calculation in favour of the numerical, using FINESSE [24] to simulate the RIN requirement. This is done by simulating the quantum noise at the BHD detection port, finding the transfer function of input laser power noise at the BP to detection port, and dividing quantum noise by the transfer function then by the input laser power.

The transfer functions from the input laser amplitude fluctuations to the BHD readout port with homodyne angle $\pi/2$ and $\pi/4$ are shown in figure 4. And the main beam-splitter asymmetry is characterised by setting $R_{BS} = 0.501$. As we can see, the transfer functions for *co-moving* and BSAR LO options are significantly weakened compared to the main laser LO option in low frequency for both homodyne angles. Another feature that we notice is the difference between the two readout quadratures in high frequency for three LO options. That can be understood from the equation (27), since for phase quadrature readout, the transfer function of the amplitude quadrature noise is just proportional to \mathcal{K}_{sym} , which decrease in high frequency according to equation (17). However, on an alternative homodyne angle as shown in equation (23) and (24), the amplitude noise gets coupled to the readout constantly and dominates in high frequency. From the two equations, we can also understand the dip at a specific frequency that indicates a cancellation between the frequency dependent back action noise and the constantly coupled amplitude noise for the case $\phi = \frac{\pi}{4}$. We note that the gap between *co-moving* LO option and BSAR LO option comes from the relatively weak LO power from BSAR as shown in table 1. In this experimental set up, the power of the laser we use is 1.7 W and the AR reflection is 100 ppm. So that the presentation for BSAR option here is only on the state of principle illustration but not for realistic implementation for this experiment.

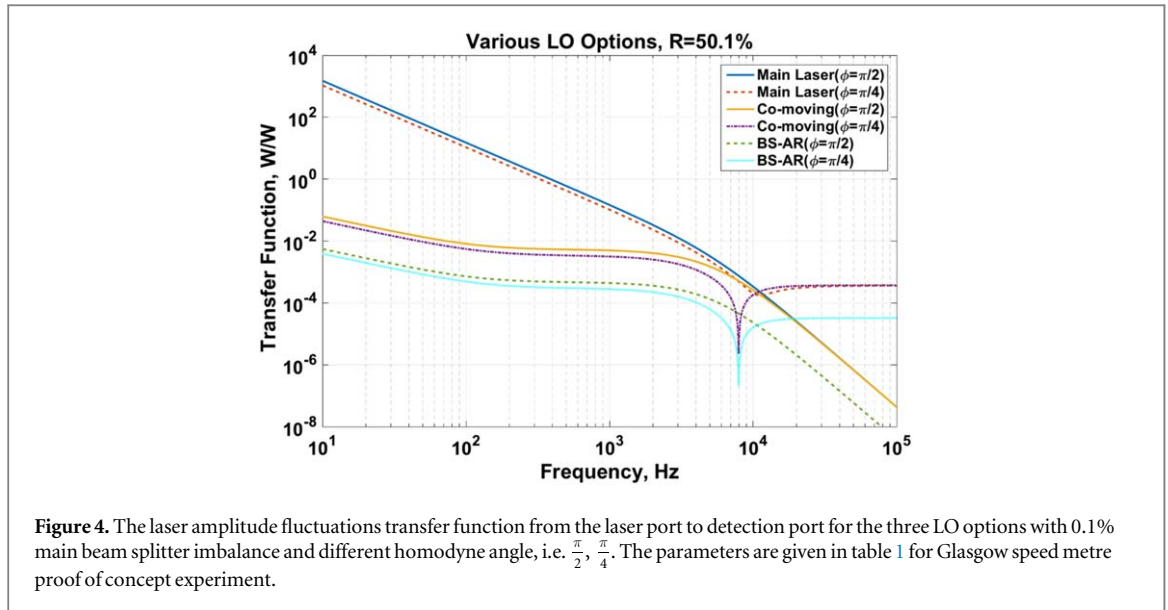
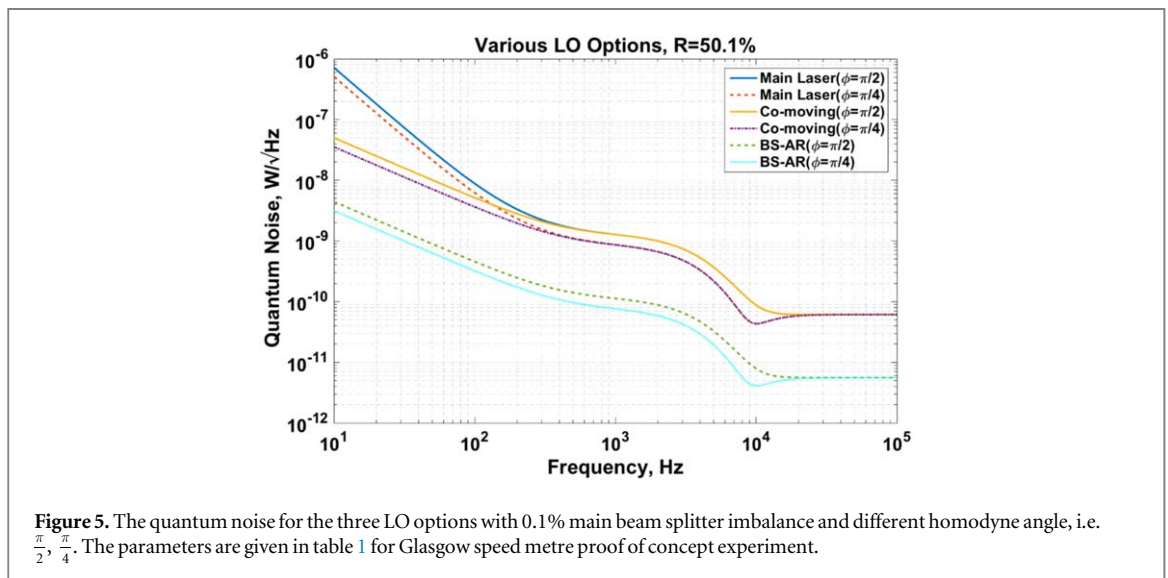
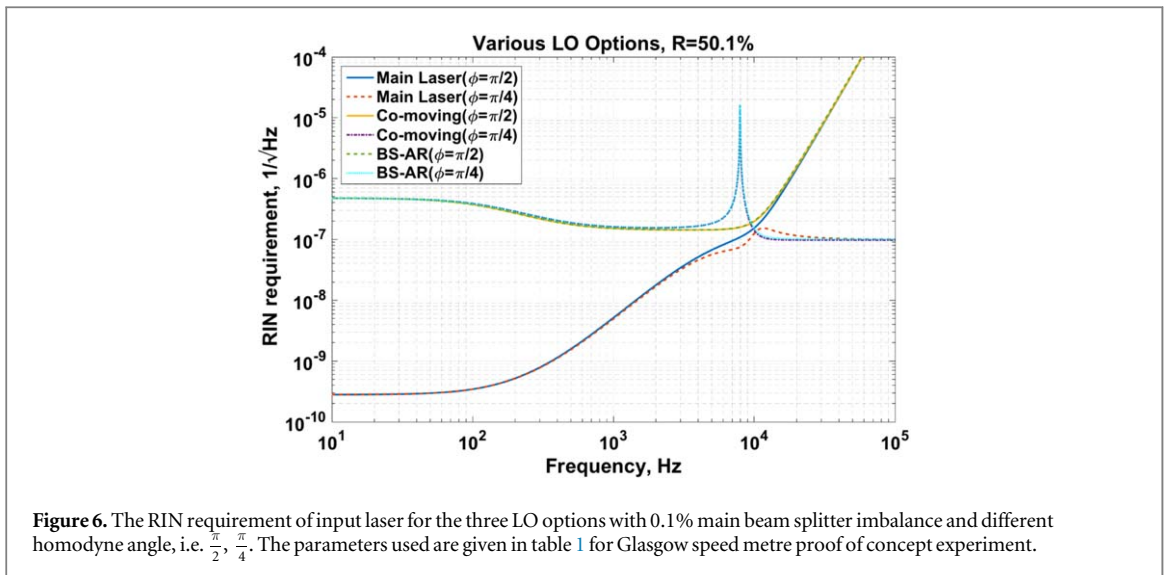


Table 1. Parameters of the Glasgow SSM experiment.

Parameter	Value
Arm cavity length L	1.3 m
Optical power P	1.7 W at beam splitter, ~ 1 kW in the arms
Arm cavity round trip loss	≤ 25 ppm
Optic mass m	Arm cavity input test mass (ITM) 860 mg, arm cavity end test mass (ETM) 100 g
Transmissivities T and reflectivities R	Central beamsplitter, $R_{BS} = T_{BS} = 0.5$, ITM, $T_{ITM} = 700$ ppm
Main Laser LO and <i>co-moving</i> LO power	10 mW
BSAR LO power	0.078 mW
Main readout	Balanced homodyne detector with suspended optical local oscillator path



The figure 5 shows the quantum noise for the three LO options with different readout quadratures. Figure 6 shows the RIN requirement. As expected, the RIN requirement get relaxed by three orders of magnitude below 100 Hz by selecting co-moving or BSAR LO options.



4. Summary

Speed-metre configurations of GW interferometers are known to provide a significant improvement of quantum noise limited sensitivity at low frequencies because by suppression of quantum back-action noise using QND measurement of speed [28, 32]. This advantage increases the signal-to-noise ratio (SNR) of speed-metre-based GW detectors for compact binary coalescences by at least two orders of magnitude if compared to the equivalent Michelson interferometer in the quantum-noise-limited case [33]. Zero-area Sagnac interferometer is one of the possible ways to realise the GWD based on speed-metre principle. However it was shown [21] that, in a non-ideal realistic case of asymmetric beam splitter, the fluctuations of the laser pump couple into the readout port of the interferometer, thereby creating an excess radiation pressure noise that significantly worsens the QNLS of speed metre interferometer and hence its SNR. In this work, we demonstrate that using a balanced homodyne readout scheme with a particular choice of the LO option this detrimental effect can be almost completely attenuated.

Picking the LO beam from the reflected light at the pumping port of the interferometer (the *co-moving* LO option), or from the direct reflection off the main beam splitter's AR coating (the BSAR LO option), one can significantly reduce the magnitude of the transfer function of the laser fluctuations from the pumping port to the readout one and qualitatively change its frequency dependence at low frequencies. We show analytically that this partial cancellation of laser fluctuations stems from the very nature of the BHD scheme that is inherently insensitive to any common variations of light phase in LO and signal beam of the BHD driven by input laser fluctuations. We further confirm our analytical findings by numerical simulation of the Glasgow proof-of-principle speed-metre interferometer set-up and estimating the relative laser intensity noise requirements for it. Our simulation shows that at frequency of 100 Hz the RIN decreases by 3 orders of magnitude, from $4 \times 10^{-10}/\sqrt{\text{Hz}}$ to $4 \times 10^{-7}/\sqrt{\text{Hz}}$ if the *co-moving* or BSAR LO option is chosen versus the conventional *direct* pick-off of the LO beam from the main laser. It is worth noting here that these 3 orders of magnitude mean reducing the RIN requirement from a very challenging value which is beyond the best achieved so far [34–36] to a value which is easily achievable.

This feature of Sagnac interferometer can, in principle, be expanded to any scheme of speed-metre interferometer that uses the Sagnac-type way of performing the velocity measurement, where signal sidebands co-propagate with the carrier light throughout the main interferometer, including the polarisation-based speed metres [15, 16, 33]. Hence, we report here the method that solves the challenges originating from beam splitter asymmetry of a real speed-metre interferometer setup by using a balanced homodyne readout scheme with a particular choice of a LO beam.

Acknowledgments

The authors are very grateful to our colleagues from the LIGO-Virgo Scientific Collaboration (LVC) for illuminating discussions and invaluable feedback on the research presented in this paper. TZ, SS, PD, JSH, EAH, SSL, SH and SLD were supported by the European Research Council (ERC- 2012-StG: 307245). SLD was supported by the Lower Saxonian Ministry of Science and Culture within the frame of Research Line

(Forschungslinie) QUANOMET Quantum- and Nano-Metrology. The work of EK and FYK was supported by the Russian Foundation for Basic Research Grants 14-02-00399 and 16-52-10069. FYK was also supported by the LIGO NSF Grant PHY-1305863. SS was supported by the European Commission Horizon 2020 Marie-Skłodowska-Curie IF Actions, grant agreement 658366. PD, JB were supported by STFC consolidated grant, ST/N005422/1.

ORCID iDs

E Knyazev  <https://orcid.org/0000-0002-9621-5967>

A S Bell  <https://orcid.org/0000-0003-1523-0821>

S L Danilishin  <https://orcid.org/0000-0001-7758-7493>

References

- [1] Abbott B P *et al* 2016 Observation of gravitational waves from a binary black hole merger *Phys. Rev. Lett.* **116** 061102
- [2] Abbott B P *et al* 2016 Gw151226: observation of gravitational waves from a 22-solar-mass binary black hole coalescence *Phys. Rev. Lett.* **116** 241103
- [3] Abbott B P *et al* 2017 Gw170104: observation of a 50-solar-mass binary black hole coalescence at redshift 0.2 *Phys. Rev. Lett.* **118** 221101
- [4] Abbott B P *et al* 2017 GW170814: a three-detector observation of gravitational waves from a binary black hole coalescence *Phys. Rev. Lett.* **119** 141101
- [5] Abbott B P *et al* 2017 GW170608: observation of a 19 solar-mass binary black hole coalescence *Astrophys. J. Lett.* **851** L35
- [6] Abbott B P *et al* 2017 GW170817: observation of gravitational waves from a binary neutron star inspiral *Phys. Rev. Lett.* **119** 161101
- [7] Abbott B P *et al* 2017 Multi-messenger observations of a binary neutron star merger *Astrophys. J. Lett.* **848** L12
- [8] Harry G M and (The LIGO Scientific Collaboration) 2010 Advanced LIGO: the next generation of gravitational wave detectors *Class. Quantum Grav.* **27** 084006
- [9] Abbott B P *et al* 2018 Prospects for observing and localizing gravitational-wave transients with advanced LIGO, advanced Virgo and KAGRA *Living Rev. Relativ.* **21** 3
- [10] Braginsky V B and Khalili F J 1990 Gravitational wave antenna with QND speed meter *Phys. Lett. A* **147** 251–6
- [11] Braginsky V B, Gorodetsky M L, Khalili F Y and Thorne K S 2000 Dual-resonator speed meter for a free test mass *Phys. Rev. D* **61** 044002
- [12] Braginsky V B and Khalili F Y 1996 Quantum nondemolition measurements: the route from toys to tools *Rev. Mod. Phys.* **68** 1–11
- [13] Purdue P and Chen Y 2002 Practical speed meter designs for quantum nondemolition gravitational-wave interferometers *Phys. Rev. D* **66** 122004
- [14] Chen Y 2003 Sagnac interferometer as a speed-meter-type, quantum-nondemolition gravitational-wave detector *Phys. Rev. D* **67** 122004
- [15] Danilishin S L 2004 Sensitivity limitations in optical speed meter topology of gravitational-wave antennas *Phys. Rev. D* **69** 102003
- [16] Wang M, Bond C, Brown D, Brückner F, Carbone L, Palmer R and Freise A 2013 Realistic polarizing sagnac topology with dc readout for the Einstein telescope *Phys. Rev. D* **87** 096008
- [17] Huttner S H *et al* 2017 Candidates for a possible third-generation gravitational wave detector: comparison of ring-Sagnac and sloshing-Sagnac speedmeter interferometers *Class. Quantum Grav.* **34** 024001
- [18] Knyazev E, Danilishin S, Hild S and Khalili F Y 2017 Speedmeter scheme for gravitational-wave detectors based on EPR quantum entanglement *Phys. Lett. A* **382** 2219–25
- [19] Sun K-X, Fejer M M, Gustafson E and Byer R L 1996 Sagnac interferometer for gravitational-wave detection *Phys. Rev. Lett.* **76** 3053–6
- [20] Beyersdorf P T, Fejer M M and Byer R L 1999 Polarization sagnac interferometer with a common-path local oscillator for heterodyne detection *J. Opt. Soc. Am. B* **16** 1354–8
- [21] Danilishin S L, Gräf C, Leavey S S, Hennig J, Houston E A, Pascucci D, Steinlechner S, Wright J and Hild S 2015 Quantum noise of non-ideal Sagnac speed meter interferometer with asymmetries *New J. Phys.* **17** 043031
- [22] Sun K-X, Gustafson E K, Fejer M M and Byer R L 1997 Polarization-based balanced heterodyne detection method in a Sagnac interferometer for precision phase measurement *Opt. Lett.* **22** 1359–61
- [23] Sun K-X, Fejer M M, Gustafson E K and Byer R L 1997 Balanced heterodyne signal extraction in a postmodulated Sagnac interferometer at low frequency *Opt. Lett.* **22** 1485–7
- [24] Freise A, Heinzl G, Lück H, Schilling R, Willke B and Danzmann K 2004 Frequency-domain interferometer simulation with higher-order spatial modes *Class. Quantum Grav.* **21** S1067
- [25] Caves C M and Schumaker B L 1985 New formalism for two-photon quantum optics: I. Quadrature phases and squeezed states *Phys. Rev. A* **31** 3068–92
- [26] Caves C M and Schumaker B L 1985 New formalism for two-photon quantum optics: II. Mathematical foundation and compact notation *Phys. Rev. A* **31** 3093–111
- [27] Kimble H J, Levin Y, Matsko A B, Thorne K S and Vyatchanin S P 2002 Conversion of conventional gravitational-wave interferometers into QND interferometers by modifying their input and/or output optics *Phys. Rev. D* **65** 022002
- [28] Danilishin S L and Khalili F Y 2012 Quantum measurement theory in gravitational-wave detectors *Living Rev. Relativ.* **15** 5
- [29] Steinlechner S *et al* 2015 Local-oscillator noise coupling in balanced homodyne readout for advanced gravitational wave detectors *Phys. Rev. D* **92** 072009
- [30] Zhang T *et al* 2017 Effects of static and dynamic higher-order optical modes in balanced homodyne readout for future gravitational waves detectors *Phys. Rev. D* **95** 062001
- [31] Gräf C *et al* 2014 Design of a speed meter interferometer proof-of-principle experiment *Class. Quantum Grav.* **31** 215009
- [32] Chen Y, Danilishin S L, Khalili F Y and Müller-Ebhardt H 2011 QND measurements for future gravitational-wave detectors *Gen. Relativ. Gravit.* **43** 671–94
- [33] Danilishin S L, Knyazev E, Voronchev N V, Khalili F Y, Gräf C, Steinlechner S, Hennig J-S and Hild S 2018 A new quantum speed-meter interferometer: measuring speed to search for intermediate mass black holes *Light: Sci. Appl.* **7** 11

- [34] Seifert F, Kwee P, Heurs M, Willke B and Danzmann K 2006 Laser power stabilization for second-generation gravitational wave detectors *Opt. Lett.* **31** 2000–2
- [35] Kwee P, Willke B and Danzmann K 2011 New concepts and results in laser power stabilization *Appl. Phys. B* **102** 515–22
- [36] Junker J, Oppermann P and Willke B 2017 Shot-noise-limited laser power stabilization for the AEI 10 m prototype interferometer *Opt. Lett.* **42** 755–8